Growth and characterization of fullerene nanocrystals on NaCl/Au(111)

Rossel, F ; Pivetta, M ; Patthey, F ; Cavar, E ; Seitsonen, A P ; Schneider, W-D

Abstract: The growth of fullerene nanocrystals, composed of only C(60), only C(70), or a mixture of both fullerenes, has been investigated by scanning tunneling microscopy (STM). The nanocrystals, formed on a NaCl ultrathin layer partially covering a Au(111) surface, have characteristic truncated-triangular or hexagonal shapes, with lateral size up to 100 nm and a typical height of two to four molecular layers. This growth mode differs considerably from the ones observed on metallic surfaces. STM images with bias-dependent submolecular resolution reveal the spatial distribution of the electronic density originating from the molecular orbitals. A comparison of the experimental results with first-principles density functional theory calculations allows us to unambiguously determine the orientation and the nature of individual fullerene molecules in the surface layer of the nanocrystals.

DOI: https://doi.org/10.1103/PhysRevB.84.075426

Growth and characterization of fullerene nanocrystals on NaCl/Au(111)

Frédéric Rossel,[1] Marina Pivetta,[1] François Patthey,[1] Elizabeta Ćavar,[1,2] Ari P. Seitsonen,[3] and Wolf-Dieter Schneider[1]

[1] *Ecole Polytechnique Fédérale de Lausanne (EPFL), Institut de Physique de la Matière Condensée, CH-1015 Lausanne, Switzerland*
[2] *University of Konstanz, Fachbereich Physik, D-78457 Konstanz, Germany*
[3] *Institut für Physikalische Chemie, University of Zürich, Winterthurerstrasse 190, CH-8057 Zurich, Switzerland*

(Dated: June 20, 2011)

The growth of fullerene nanocrystals, composed of only C_{60}, only C_{70}, or of a mixture of both fullerenes, has been investigated by Scanning Tunneling Microscopy (STM). The nanocrystals, formed on a NaCl ultrathin layer partially covering a Au(111) surface, have characteristic truncated-triangular or hexagonal shapes, with lateral size up to 100 nm and a typical height of two to four molecular layers. This growth mode differs considerably from the ones observed on metallic surfaces. STM images with bias-dependent submolecular resolution reveal the spatial distribution of the electronic density originating from the molecular orbitals. A comparison of the experimental results with first principle Density Functional Theory (DFT) calculations allows us to unambiguously determine the orientation and the nature of individual fullerene molecules in the surface layer of the nanocrystals.

PACS numbers: 68.55.Ac 68.37.Ef

I. INTRODUCTION

Since their discovery in 1985[1] fullerene molecules have been investigated by numerous experimental and theoretical tools to get insight into the origin of their unique physical and chemical properties[2]. Especially, Scanning Tunneling Microscopy (STM)[3] has been proven to be very useful in elucidating at molecular and sub-molecular spatial resolution the structural and electronic properties of C_{60} grown on different metallic[4–14] and semiconducting substrates[15,16]. The majority of these studies concentrate on the interaction of single molecules or molecular monolayers (ML) with the substrate. For example, on bare gold surfaces, the fullerene molecules aggregate into islands, mostly of 1 ML height, nucleating at gold step edges and spreading over both, upper and lower terraces[5,7,8,17,18].

A different behavior is observed in Atomic Force Microscopy (AFM) studies for the growth of fullerenes on dielectric NaCl and of KBr substrates. In this case, owing to a subtle balance of surface energies and dewetting phenomena[19–21], the fullerene molecules grow in a three-dimensional (3D) fashion and form nanocrystals. Similar results have been obtained for other molecules such as bimolecular perylenetetracarboxylic diimide (PTCDI) and BDATB on NaCl on vicinal Au surfaces[22]. On the other hand, for porphyrines the formation of 2D ordered epitaxial molecular monolayers on NaCl has been observed[23], which was attributed to a decreasing van der Waals interaction with increasing number of alkali halide layers and additional charge transfer to the underlying Ag(001) metal substrate. Furthermore, a direct comparison of SnPc growth on Au(111) and on NaCl/Au(111) showed that on Au(111) SnPc is adsorbed with the molecular plane parallel to the surface and grows in a Stranski-Krastanov mode, while on NaCl, Vollmer-Weber growth of three-dimensional molecular nanocrystals occurs[24]. Here, the intermolecular interactions dominate over the molecule-NaCl coupling.

In this communication, we report on a STM study of the nucleation and growth of fullerenes on NaCl layers deposited on a Au(111) surface. On the NaCl layers, the growth mode is different from the one observed on the bare metal substrate, owing to the different adsorption energies[19–21] : the fullerene molecules form nanocrystals with a minimal height of 2 ML. Furthermore, similarly shaped nanocrystals are obtained after co-deposition of C_{60} and C_{70} molecules, showing again that on these dielectric substrates the intermolecular interactions prevail over the fullerene-substrate coupling. The spatial resolution of the STM together with DFT calculations allow us to identify individual fullerene molecules and their packing in the topmost layer, for both, C_{60} and C_{70} nanocrystals as well as for mixed C_{60} and C_{70} nanocrystals. While orientational ordering is observed for the pure C_{60} and C_{70} nanocrystals, in the surface layer of the mixed ones the orientational ordering of the molecules is disturbed. The fullerene molecules in the surface layer of the nanocrystals tend to arrange in configurations where electron-poor regions on one molecule face electron-rich regions on the adjacent molecule.

II. EXPERIMENTAL DETAILS AND THEORETICAL METHODS

The Au(111)/mica substrate was prepared by standard argon-ion sputtering and subsequent annealing cycles in a vacuum chamber with a base pressure in the low 10^{-10} mbar range. First, NaCl was deposited onto the gold sub-

strate from a Knudsen cell. Subsequently, the fullerene molecules were sublimed from a heated tantalum crucible onto the NaCl covered Au(111) substrate[25]. For mixed C_{70} and C_{60} nanocrystals, successive as well as simultaneous depositions of C_{70} and C_{60} fullerenes onto a NaCl covered Au(111) substrate have been performed using two different crucibles, each one containing a high purity powder of one type of molecules[26]. During both evaporation cycles, the sample was held at room temperature and only subsequently cooled down to 50 K in order to perform the measurements. The experiments were carried out in a home-built STM[27], using etched W tips.

We performed Density Functional Theory (DFT) calculations for the C_{60} and C_{70} molecules, and a one-dimensional row and two-dimensional layer of molecules. We employed the plane wave basis up to a cut-off energy 50 Ry to expand the Kohn-Sham orbitals. For the cluster calculations we used the CPMD code[28] for the isolated molecule with the PBE0 hybrid functional as the exchange-correlation term[29] in order to obtain a stronger localization of the Kohn-Sham states and a more accurate correspondence between the Kohn-Sham eigenvalues and the real electronic spectrum. For the calculations of the 1D- and 2D-periodic structures we used the code Quantum ESPRESSO[30] with the van der Waals density functional[31] to describe the weak interaction between the closed-shell fullerene molecules better than the more traditional Local Density (LDA) or Generalised Gradient Approximation (GGA). In the non-periodic directions sufficient amount of vacuum, typically over 12 Å, was used. We took the experimentally found value (see below) $r = 1.05$ nm as the lattice constant, or distance between the centres of the molecules. One and two molecules in the super-cell were simulated in the one-dimensional rows and two-dimensional layer, respectively. The molecules were ordered standing on a pentagon fixed into a plane.

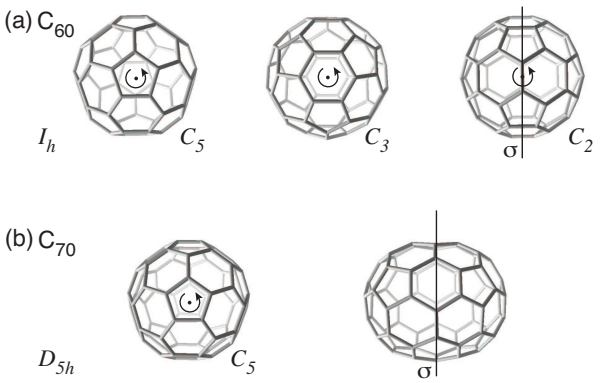

FIG. 1: a) The C_{60} molecule (I_h symmetry); the symmetry operations C_5, C_3, C_2, and σ are indicated, (plus inversion). b) The C_{70} molecule (D_{5h} symmetry); the symmetry operations C_5 and the mirror plane σ perpendicular to the fivefold axis (the inversion symmetry is lost).

III. RESULTS AND DISCUSSION

A. Basic considerations of fullerene adsorption on Au(111) and on NaCl/Au(111)

Upon adsorption on Au(111) at room temperature, NaCl forms large (with the size of a few squared micrometers) (100)-terminated islands starting with two or three atomic layers[25,32]. Figure 2 shows an STM topography of such a triple layer NaCl island on Au(111). In the left part of the figure (dark contrast) the herringbone reconstruction of the bare gold surface is clearly visible[25,26,33,34]. In the outermost atomic layer of the Au(111) surface, 23 atoms are arranged over 22 bulk lattice sites, resulting in a contraction of the interatomic distance from 0.289 nm (bulk value) to 0.275 nm along the $\langle 1\bar{1}10\rangle$ direction. This mismatch between the top and second layer leads to a $22 \times \sqrt{3}$ rectangular overlayer structure with alternating, hexagonal close packed (hcp) and face centered cubic (fcc) domains, separated by soliton walls. Due to the threefold orientational degeneracy of the Au(111) surface the direction of these boundaries periodically rotates by 120°, forming a characteristic herringbone (chevron) pattern[33]. As illustrated in the right part of Fig. 2, this herringbone reconstruction of the gold surface is preserved, giving rise to the apparent herringbone-like topography on the NaCl layer. This phenomenon is related to the observed carpet-like overgrowth behavior of NaCl films[35]. The first two layers have an apparent height of 0.18 ± 0.01 nm (the physical thickness is 0.28 nm), whereas the apparent height of the third and fourth layers is approximatively 0.17 nm and 0.16 nm, respectively. This non-linearity of the apparent height of NaCl multilayers with the number of layers is typical for insulating films and originates from the difference of the apparent tunneling barrier formed by NaCl layers of different thickness[36,37]. Note that the values of the apparent height may differ substantially depending on the tip state or the bias voltage used for scanning[22,38]. Table I summarizes the measured apparent heights observed for the investigated systems in the present study.

Figure 3 shows a typical STM image of a sample measured after deposition of C_{60} molecules onto a Au(111) substrate partially covered with a NaCl layer. The same overall surface morphology is observed for deposition of C_{70} molecules, or for co-deposition of both fullerenes. The topography image reveals a complex system composed of bare Au(111) surface areas, C_{60} islands grown on Au(111), extended ultrathin NaCl islands on Au(111), and C_{60} nanocrystals grown on the NaCl-covered surface. The fullerene nanocrystals clearly occupy preferential nucleation sites: NaCl-covered substrate step edges, defects of the NaCl film (protrusions or vacancies), and NaCl-adlayer step edges. This preferred nucleation at these NaCl specific locations has been found previously in AFM studies for C_{60} islands grown on KBr

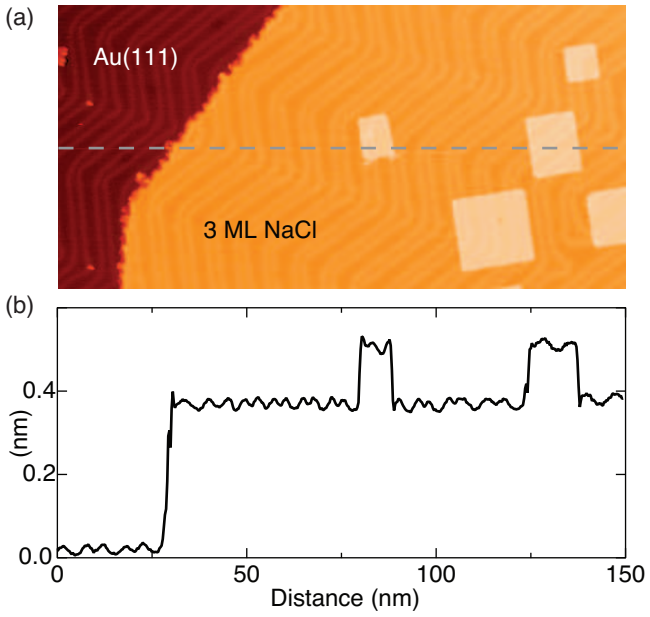

FIG. 2: (color online) STM topography of a NaCl triple layer island on Au(111). The bare gold surface is visible in the left part of the image. The herringbone reconstruction of Au(111) below the ultrathin NaCl film is preserved. On top of this island double layer rectangular NaCl patches are observed, as indicated in the height profile shown in (b). Tunneling parameters: $V = -1.5$ V, $I = 20$ pA.

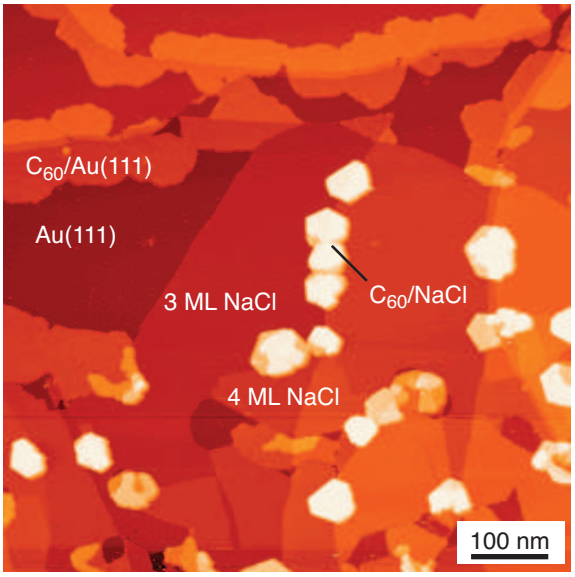

FIG. 3: (color online) Overview STM image showing the growth of C_{60} on Au(111) and on NaCl/Au(111). Regions of bare gold, of C_{60}/Au(111), of NaCl/Au(111), as well as C_{60} nanocrystals grown on NaCl are identified. Tunneling parameters: $V = -3.0$ V, $I = 20$ pA.

and NaCl single crystal surfaces[19,20] and were attributed to the large molecular diffusion length on such alkali halide substrates[19,39]. The surface of the nanocrystals is not necessarily flat, it follows the profile of the underlying topography, e. g., reflects step edges or the presence of an additional NaCl adlayer. Moreover, the topmost layer can be complete or only partially occupied by fullerenes. The fullerene nanocrystals show characteristic truncated-triangular or hexagonal shapes. Most of them have a compact configuration, although branched nanocrystals[19,20] have also been occasionally observed. In addition, the shape of the fullerene nanocrystals can also be influenced by the local environment, such as the presence of step edges on the substrate. For the present growth conditions, the fullerene nanocrystals have a typical lateral size between 20 to 100 nm and a thickness between 2 and 4 molecular layers.

B. C_{60} nanocrystals

The C_{60} molecule is composed of 60 carbon atoms, arranged in 12 pentagons and 20 hexagons, forming a truncated icosahedron with a diameter of 0.71 nm^2, as shown in Fig. 1(a). Each pentagon is surrounded by five hexagons. The C-C bonds separating two hexagons have a substantial double bond character while the pentagon C-C bonds have a prevalent single bond character[2]. At room temperature, C_{60} crystallizes into a face centered cubic (fcc) lattice with four equivalent molecules per conventional unit cell (see Ref.[2] and references cited therein). As the molecules are rotating rapidly about their lattice positions with three degrees of rotational freedom and independently of each other, there is no orientational order. At a temperature below approximatively 260 K, the C_{60} molecules lose two of their three degrees of rotational freedom, so that the residual rotational motion occurs only around the four $\langle 111 \rangle$ directions. The molecules are still at the same relative positions as in the room temperature phase, but the four positions per conventional unit cell of an fcc lattice have become inequivalent due to four distinct molecules rotating about four different $\langle 111 \rangle$ directions[40,41]. The structure thus becomes simple cubic (sc) with four distinct molecules per unit cell. When the temperature is lowered further, additional ordering of the molecules occurs as the rotational motion becomes hindered, whereby adjacent molecules develop strongly correlated orientations. There are two energetically, nearly degenerate, orientational variants for each molecule. In the idealized ordered structure, the relative orientation of adjacent molecules is stabilized by aligning an electron-rich bond common to two hexagons on one C_{60} molecule opposite to an electron-poor pentagonal face of an adjacent C_{60} molecule[42–45]. The high symmetry of the C_{60} molecule permits to optimize these interactions identically for all 12 neighbours. In the second ordered structure (called the "defect structure"), the orientation of adjacent molecules is stabilized by aligning

	1 ML (nm)	2 ML (nm)	3 ML (nm)	4 ML (nm)
NaCl/Au(111)	–[a]	0.18 ± 0.01	0.34 ± 0.01	0.51 ± 0.03
C_{60}/Au(111)	≈0.65	–	–	–
C_{70}/Au(111)	≈0.7	–	–	–
C_{60}/NaCl/Au(111)	1.05 ± 0.05	1.95 ± 0.05	2.7 ± 0.05	3.7 ± 0.1
C_{70}/NaCl/Au(111)	–	2.3 ± 0.05	3.3 ± 0.1	4.2 ± 0.1

[a] The growth of NaCl layers starts with a double layer.

TABLE I: Summary of the measured apparent heights observed for the investigated systems. The uncertainties given take into account the statistics.

the bond common to two hexagons on one C_{60} molecule opposite to an electron-poor hexagonal face of an adjacent C_{60} molecule. The energy difference between these two orientations was found to be 11 meV[46]. The orientational alignment begins to set in at a temperature between 165 and 90 K(Ref.[2]). In the low temperature phase below 90 K, the rotational motion of individual molecules is frozen, and an orientational glass state is formed[44]. The superstructure is reported to be a fcc crystal structure with lattice parameter $2a_0$ ($a_0 = 1.42$ nm)[42,47,48]. The orientational glass state has the following characteristics. Below 90 K the C_{60} molecules are frozen into a glassy phase (or rotational frozen phase), where the rotational freedom of the molecules is lost, each molecule randomly occupies one of the two orientation-dependent local energy minima[44,48].

Figure 4(a) shows a typical STM topography of several C_{60} nanocrystals nucleated at a NaCl step edge. The line profile extracted from the image in Fig. 4(a) and reported in (b) follows from left to right the apparent height of a molecular island grown on the bare Au(111) surface, a C_{60} nanocrystal on NaCl, and of the ultrathin NaCl spacer layer. The apparent height of the C_{60} nanocrystal with respect to the NaCl layer is 1.95 ± 0.05 nm, corresponding to a nanocrystal with a height of two layers of C_{60} molecules. Nanocrystals with an apparent height of 2.7 ± 0.05 nm, as the one with the bright contrast shown in the right part of Fig. 4(a), and 3.7 ± 0.1 nm have also been observed, corresponding respectively to three and four molecular layers, as previously reported[32]. A nanocrystal with an apparent height of 1.05 ± 0.05 nm, formed by a single layer of molecules, has been observed only in one experiment. The line profile of the monolayer islands grown on the bare Au surface indicates an apparent height of approximately 0.65 nm. This value is in agreement with the results reported for C_{60} on Au(111), with a weak dependence on the bias voltage[49].

A close-up view of the surface of a C_{60} nanocrystal, shown in Fig. 5(a), demonstrates that the molecules are arranged in a close-packed structure. The nearest-neighbor distance, deduced from the line-scan presented in Fig. 5(b), is 1.05 ± 0.05 nm, close to the value reported for crystalline C_{60} (1.002 nm [Ref. 2]). Therefore, the fullerene nanocrystals are identified as (111)-terminated islands possessing a bulk-like fcc structure.

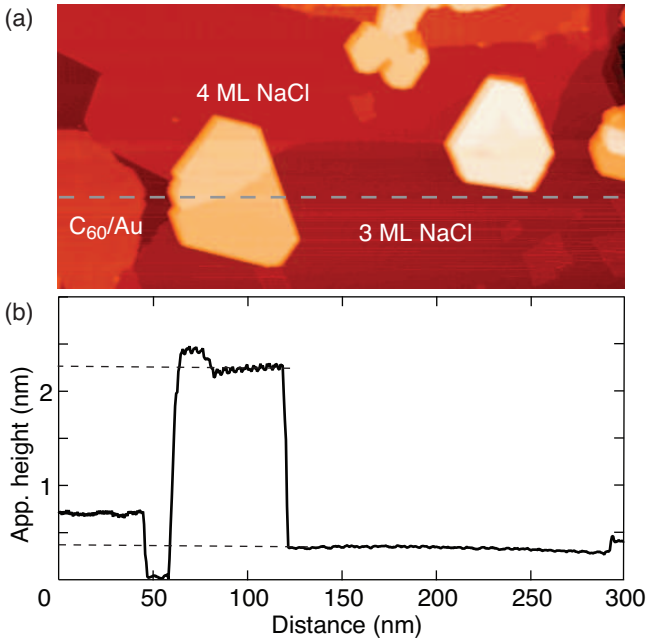

FIG. 4: (color online) a) STM image showing several C_{60} nanocrystals nucleated at a NaCl step edge. b) Line profile corresponding to the dashed line in a), showing from left to right a C_{60}/Au(111) island of 0.65 nm thickness, a part of the bare Au(111) surface around 50 nm, and a 2 ML-high C_{60} nanocrystal on NaCl. The thickness of the NaCl layers is indicated. The non-uniform height of the $C_{60}/NaCl$ nanocrystal originates from a step in the underlying NaCl substrate. Tunneling parameters: $V = -3.0$ V, $I = 20$ pA.

Figure 6(a) and (b) show high resolution STM images of the surface layer of a C_{60} nanocrystal for two bias polarities. Figure 6(a) with a bias voltage of +2 V shows the unoccupied molecular orbitals, while Fig. 6 (b), acquired on the same area with a bias voltage of –2.8 V, shows the occupied molecular orbitals of C_{60} molecules. Three different projections of the orbitals depending on the molecular orientations are found. As expected for measurements performed at a temperature of 50 K, the orientations of the molecules are stable in time, since the molecules are found in an orientational glass state[44]. The different observed molecular orientations, shown in Fig. 6(c, top row), could be identified by comparing

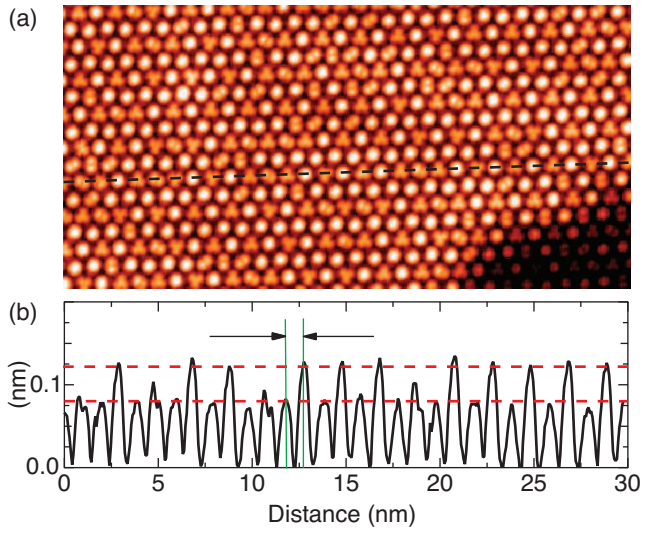

FIG. 5: (color online) a) Close-up view of the surface layer of a 2 ML thick C_{60} nanocrystal, showing the close-packed arrangement of the molecules. b) Line profile corresponding to the dashed line in (a). The nearest-neighbor distance is 1.05 nm. Tunneling parameters: $V = +2.0$ V, $I = 20$ pA.

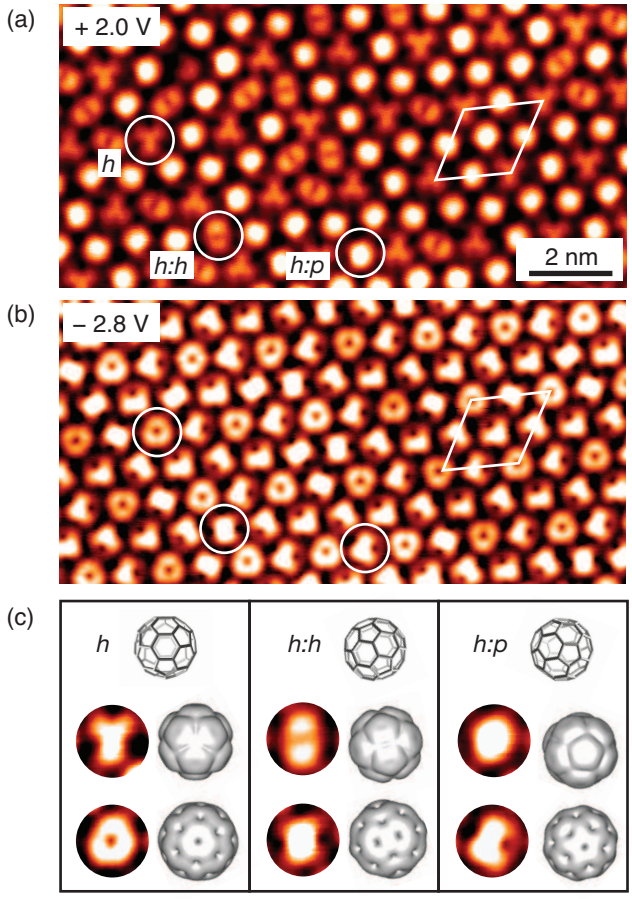

FIG. 6: (color online) High resolution STM images revealing unoccupied (a) and occupied (b) molecular orbitals of C_{60} molecules on the surface layer of a nanocrystal. c) Top row: Corresponding molecular orientations with hexagon (h), hexagon–hexagon (h:h) and hexagon-pentagon (h:p) facing the STM tip. Second and third row: Comparison of the STM topography of single molecules (high-lighted by white circles in (a, b)) with DFT calculations for the lowest unoccupied (LUMO) and highest occupied (HOMO) molecular orbitals, respectively. A typical unit cell of the long-range orientational pattern is indicated by the white parallelograms in (a, b). Tunneling parameters: (a) $V = +2.0$ V, $I = 20$ pA; (b) $V = -2.8$ V; $I = 20$ pA.

the STM-imaged orbitals with DFT calculations for the lowest unoccupied molecular orbital (LUMO) and the highest occupied molecular orbital (HOMO) of the free molecule (Fig. 6 (c), second and third row, respectively). At positive sample bias, bright lobes correspond to pentagons of the C_{60} cage. Therefore, the three, two and single– lobe intramolecular patterns distinguished and high-lighted by white circles in Fig.6 (a,b) correspond respectively to C_{60} molecules which expose a hexagon towards the tip (denoted h), two hexagons (h:h), and a hexagon plus a pentagon (h:p). We note that the spatial mapping of the spectral density by STM[4,9,50,51] and comparisons with calculations have been reported before, see, e. g.,[4,12,17,52].

Interestingly, a certain regularity in the molecular orientation is observed. The molecular orientation corresponding to a carbon hexagon facing up (h) forms the building block of a superlattice with one C_{60} molecule with a three-lobe intramolecular pattern and three C_{60} molecules with single-lobe intramolecular patterns in each unit cell, indicated by the white parallelogram in Fig. 6(a,b). The other three molecules in such a unit cell exhibit (h:p) or (h:h) orientation with a statistical weight of about 3 to 1. For C_{60} crystallites grown on Si(100) a (2×2) superlattice, formed by a periodic arrangement of molecules with a hexagon (h) or a C-C double bond (h:h) facing up and with ordered azimuthal orientations, has been reported[48]. Our superlattice differs from the idealized ordered structure reported by Wang *et al.*[48] because we observe an additional orientation of the molecules where a hexagon plus a pentagon (h:p) face the tip. This finding points to a coexistence of the ideal and the defect structure in the present case and may indicate that the lowest energy structure, i. e., the predicted glassy orientational state, is not yet reached for the surface layer of these C_{60} nanocrystals[44,45,53]. We note that in these superlattices the C_{60} molecules tend to arrange with electron-poor regions facing electron-rich regions.

A different kind of long range orientational order within C_{60} monolayers on Au(111) was observed with low-temperature scanning tunneling microscopy[10]. A unit cell comprising 49 molecules which adopt 11 different orientations was found. It can be divided in a faulted and an unfaulted half similar to the (7×7) reconstruction of Si(111). A model was proposed which shows how the substrate induces small changes in the orientation of the C_{60} molecules. Intermolecular interactions are shown to

play a major role in stabilizing the superlattice.

C. C_{70} nanocrystals

The molecule C_{70} is the second most abundant fullerene. It has an elongated rugby-ball shape (shown in Fig. 1(b)) that can be viewed of being constructed by inserting a ring of five hexagons between two hemispherical fragments of C_{60}.

The high temperature (above 360 K) equilibrium structure of solid C_{70} grown from the vapour phase is face-centered cubic (fcc), although hexagonal closed packed (hcp) crystals can also be prepared[54–56]. In both structures the molecules are freely rotating, resulting in the absence of orientational order. Upon cooling, both the fcc and hcp materials undergo phase changes associated with progressive orientational ordering. Cooling the fcc grown crystal below 340 K results in a rhombohedral structure in which the molecules are aligned with their long axis parallel to each other and rotation occurs only around this long axis[54,57]. The transformation of the fcc structure into the rhombohedral one can be considered as a stretching of the fcc lattice along a unique [111] direction, the C_{70} molecules having their long axis parallel to this direction. Further cooling below 295 K results in a second phase transition, from the rhombohedral structure to a monoclinic one, associated with the freezing out of the remainder of the rotational disorder about the long axis of the molecule[55]. When hcp grown crystals are cooled, a transition occurs slightly above room temperature from an ideal hcp structure into a deformed hcp phase (c/a ratio of 1.82 instead of 1.63 for ideal hcp)[54]. Since the new length of the a axis (1.011 nm) is close to the center-to-center distance of two aligned C_{70} molecules, it was suggested that the long axes of the different molecules are oriented along the c axis of the hexagonal lattice and that the molecules rotate around the latter. In this structure, all node points of the basic hcp lattice are occupied by C_{70} molecules. Below approximately 270 K, the rotational motion is frozen and the structure thus becomes an orientationally ordered superstructure of the deformed hcp phase (monoclinic structure)[54].

Figure 7(a) shows a typical STM image of the surface topography after deposition of C_{70} molecules onto a gold substrate covered by an ultrathin NaCl film. The thickness of the NaCl film amounts to three atomic layers. The nanocrystals have nucleated at step edges. No difference between the preferential nucleation sites for C_{60} and C_{70} has been observed. A cut along the line indicated in Fig. 7(a) yields the profile presented in Fig. 7(b). The apparent island height is determined to be 2.3 ± 0.05 nm, indicating a thickness of two molecular layers. Nanocrystals with apparent heights of 3.3 ± 0.1 nm (3 ML) and 4.2 ± 0.1 nm (4 ML) have also been observed. The apparent height of the C_{70} monolayer island grown on the bare metal surface observed in the right part of Figure 7(a, b) is 0.7 ± 0.05 nm.

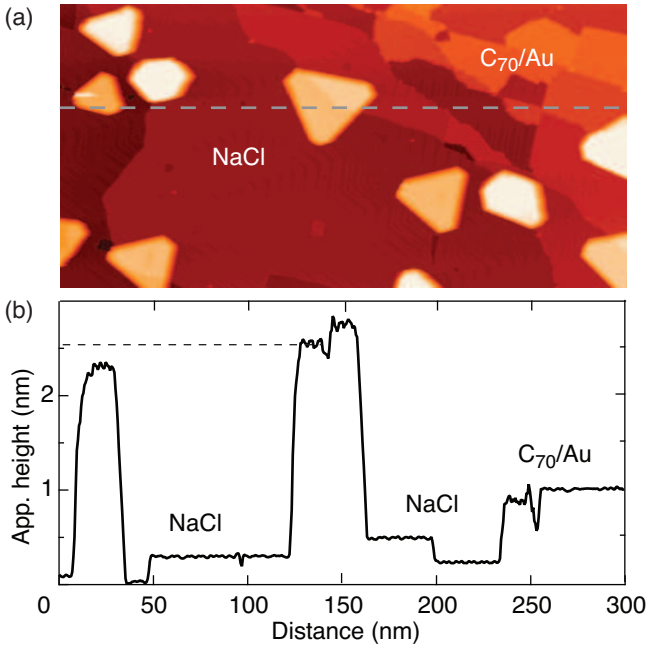

FIG. 7: (color online) a) STM image showing several C_{70} nanocrystals grown on NaCl/Au(111) and on Au(111). b) Line profile corresponding to the dashed line in (a), showing in the center a 2 ML-thick nanocrystal (2.3 nm) on NaCl and to the right a C_{70} island on bare gold (0.7 nm). Tunneling parameters: $V = -3.0$ V, $I = 20$ pA.

The fact that the apparent height of the C_{70} nanocrystal is higher than the one of equivalent C_{60} ones suggests that the C_{70} molecules stand in upright position, i.e., with their long axis perpendicular to the surface. By contrast, C_{70} molecules adsorbed on the bare gold surface assemble with their long axis parallel to the surface. Again, there is a distinct difference between the molecular growth on a metallic as compared to a dielectric substrate. A similar effect, pointing to an increased intermolecular interaction on the dielectric substrate, has been reported recently for the growth of SnPc on Au(111) and on NaCl. While on the former the molecules adsorb in a flat geometry , they adopt a tilted geometry on the latter substrate[24]. A close-up view of the surface of a C_{70} nanocrystal, displayed in Fig. 8(a,b), confirms this interpretation by showing a regular hexagonal structure with a nearest-neighbour distance of 1.06 nm, very close to the one observed in the case of C_{60}.

As shown in Fig. 8(a,b) (and also in Figs. 9(b) and Fig. 10(a)), the dark features are in fact molecules which are imaged $\approx$0.1 nm lower than the azimuthally aligned molecules. This value is too small to suggest that C_{70} molecules are missing on the top layer. On the other hand, this value is in good agreement with the difference between the longer axis of a C_{70} molecule, i.e., the axis of a fivefold rotation symmetry, and the short axes[60]. This finding suggests that the darker molecules are molecules of the topmost layer aligned with their long axis parallel

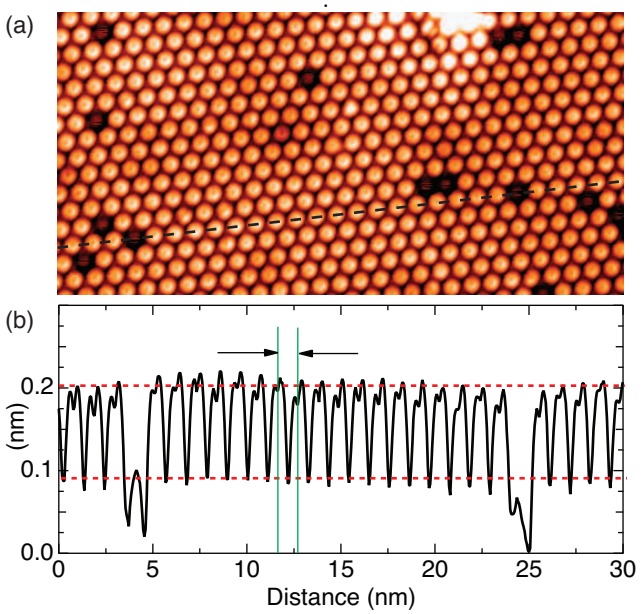

FIG. 8: (color online) a) Close-up view of the surface layer of a 3 ML thick C_{70} nanocrystal, showing the close-packed arrangement of the molecules. (b) Line profile corresponding to the dashed line in (a). The nearest-neighbor distance is 1.06 nm. Tunneling parameters: $V = +2.3$ V, $I = 50$ pA.

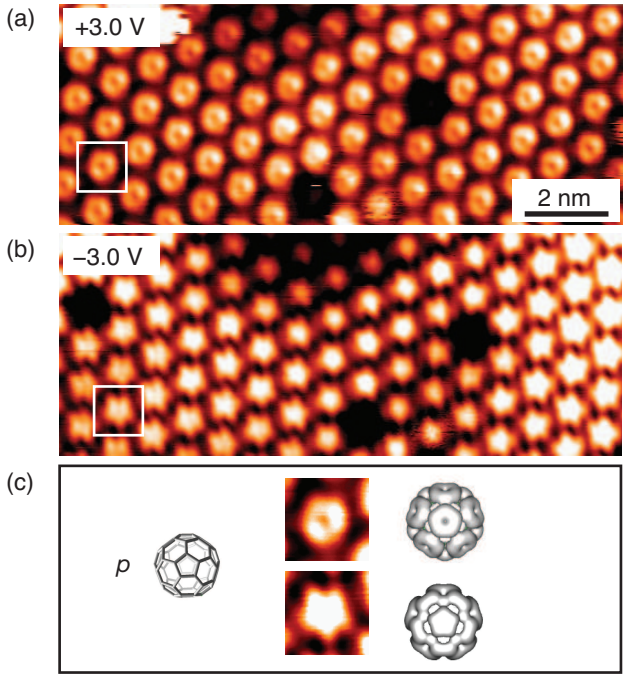

FIG. 9: (color online) High-resolution STM images revealing unoccupied (a) and occupied (b) molecular orbitals of C_{70} molecules in the surface layer of a C_{70} nanocrystal. (c) Corresponding geometry of a molecule oriented with their long axis perpendicular to the surface with a pentagon p facing the tip; comparison between observed molecular images (c, central column) and DFT calculations for the lowest unoccupied molecular orbital (LUMO) (c, right column top) and the highest occupied molecular orbital (HOMO) (c, right column bottom) for the free molecule. Tunneling parameters: (a) $V = +3.0$ V, $I = 20$ pA; (b) $V = -3.0$ V; $I = 20$ pA.

to the surface.

In the following, we focus our attention on the orientational configuration of C_{70} molecules on the top layer of nanocrystals. Figures 9(a) and (b) show high resolution STM images of the surface layer of a two molecular layers high C_{70} nanocrystal grown on an ultrathin NaCl film, revealing the unoccupied (a) and occupied (b) molecular orbitals of C_{70} molecules, respectively. The geometry of the molecules with the pentagon p facing the tip is indicated in (c), as well as the comparison between observed molecular images (c, central column) and DFT calculations for the lowest unoccupied molecular orbital (LUMO) (c, right column top) and the highest occupied molecular orbital (HOMO) (c, right column bottom) of the free molecule. The measured intermolecular distance of approximately 1.06 nm matches well the C_{70}–C_{70} nearest neighbour distance in the (111) plane of fcc grown crystals and the C_{70}–C_{70} nearest neighbour distance in the hexagonal plane of hcp grown crystals reported in the literature[54,56,58,59]. The fivefold symmetry of the molecular orbitals shown in Fig. 1(b) enables direct determination of the orientation of the molecules. The C_{70} molecules crystallize into multilayer islands with a hexagonally arranged close-packed top layer which consists of two alternating rows, marked as A and B in Fig. 10, of fixed molecules oriented with the long axis aligned along the surface normal. Note that due to the presence of defects in the surface layer, the direction of the alternating rows may vary.

By examination of high-resolution STM images as those displayed in Fig. 9(b) and Fig. 10 (a), we draw the model given in Fig. 10 (b, right). The latter schematizes the finding that C_{70} arrange in an ordered 2×1 superlattice, in which the molecules are oriented parallel to each other within the rows and differ by approximately 18° with respect to the adjacent rows. Although the observed molecular arrangement slightly differs from the energetically most favorable one predicted in Ref.[54], see Fig. 10 (b, left), the C_{70} molecules arrange with electron-poor regions (hexagonal face centers) and electron-rich regions (hexagon–hexagon edges) facing each other to a good approximation not only within one row but also between adjacent rows. In the present case, the clockwise rotation of one C_{70} molecule by $\approx 9°$ about its long axis with respect to the predicted model (rows A), and the anticlockwise rotation of one C_{70} molecule by $\approx 9°$ (rows B) are clearly resolved in each unit cell of the superlattice. A typical unit cell of the long-range orientational pattern in the surface layer of a C_{70} nanocrystal is indicated in Fig. 10(a) by the black parallelogram.

Concerning the calculations for the fullerene molecules, we consider the planar structure, where the molecules always sit on a pentagon that is fixed into a plane, simulating a flat substrate. This plane is parallel to the direction

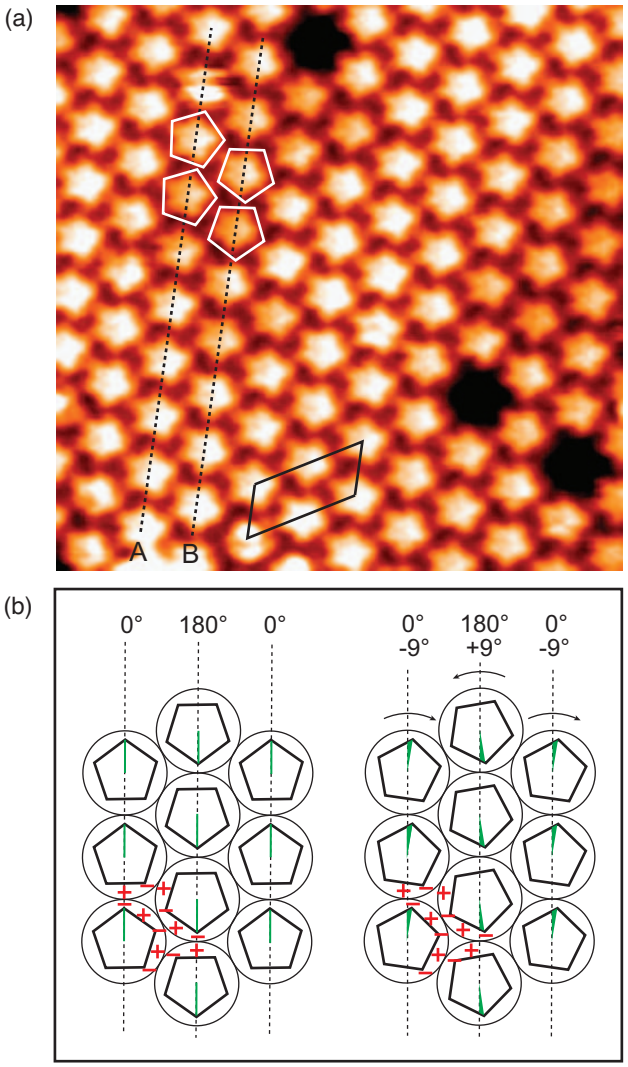

FIG. 10: (color online) (a) High-resolution STM image of the surface layer of a C_{70} nanocrystal for the occupied molecular orbitals. A, B: Two alternating rows of azimuthally aligned molecules oriented with their long axis perpendicular to the surface as deduced from their fivefold symmetry. The black parallelogram indicates a unit cell of a 2×1 superlattice. (b,left) Predicted model from Ref.[54]. (b, right) Adapted model based on the observations in (a). The "–" and "+" signs indicate electron-poor and electron-rich regions, respectively. Tunneling parameters: $V = -3.0$ V; $I = 20$ pA.

of the 1D row or the 2D plane and we let the molecules rotate in the plane away from the C_{2v} symmetry group. We obtain an angle of 5.6° together with a reduction of energy by about 18 meV per molecule (see below). For C_{70} this is qualitatively similar to the experimentally derived structural model, but the energy difference between the symmetric and rotated structure is very small. For the 1D row the binding energies per not rotated and rotated molecule are 0.390 eV and 0.401 eV, respectively, while for the 2D plane a binding energy change from 1.158 eV (not rotated) to 1.176 eV is calculated (see above). For the C_{60} molecules in a 1D row the energies are 0.306 eV (not rotated) and 0.319 eV (rotated), the angle is 6.7°. The difference between calculated and experimental rotation angles is most probably due to the model assumption of a free-standing molecular layer while in the experiment the molecules rotate on an underlying molecular layer. The energy difference between the rotated and not rotated orientations of 18 meV is larger than the thermal energy of 4 meV. This implies that the molecule is frozen in one of the two rotational states, in good agreement with the experiment.

D. Mixed C_{60}-C_{70} nanocrystals

In general, co-deposition of two molecular species usually forms multiple mixed phases and bonding structures[18]. In the past, the structure of supermolecular architectures arising from co-sublimation of C_{60} molecules and different types of flat hydrocarbons has been investigated and interesting supermolecular patterns have been observed[18,61–63]. These experiments motivated us to study, with special emphasis on the molecular orientation, the supramolecular structures within fullerene nanocrystals which may result from a mutual embedding of C_{60} and C_{70} molecules supported on a dielectric NaCl surface.

1. *Successive deposition*

Figure 11(a) depicts a typical STM image of the surface topography after successive depositions of C_{70} and C_{60} molecules, respectively, onto a NaCl covered Au(111) substrate. The line profile taken along the dashed line in (a) and shown in (b) reveals the thickness and the composition of the fullerene nanocrystal. The fullerene nanocrystals exhibit a central part composed exclusively of C_{70} molecules (indicated by the two vertical dashed lines in (b) and a rim formed by C_{60} molecules only. The apparent heights of approximately 3.3 nm (core) and 2.7 nm (rim) correspond to the ones of pure C_{70} and pure C_{60} nanocrystals, comprising three stacked molecular layers, respectively (compare Sect. III, B and C). Mixed C_{70}/C_{60} fullerene nanocrystals with a uniform shape consist of the same number of layers of both fullerene species. The fact that these samples never contained pure C_{60} nanocrystals indicates that C_{70} islands represent preferential nucleation sites for C_{60} molecules.

The smaller scale STM image displayed in Fig. 12(a) shows the surface layer of the nanocrystal displayed in Fig. 11(a) at molecular resolution. As in the case of fullerene nanocrystals composed of only one type of molecules, the C_{70}–C_{70} and C_{60}–C_{60} nearest-neighbour distances are approximately 1.05 nm, as illustrated in Fig. 12(b). Furthermore, the molecular patterns of hexagonal symmetry and the intramolecular features are similar to those observed for nanocrystals composed of

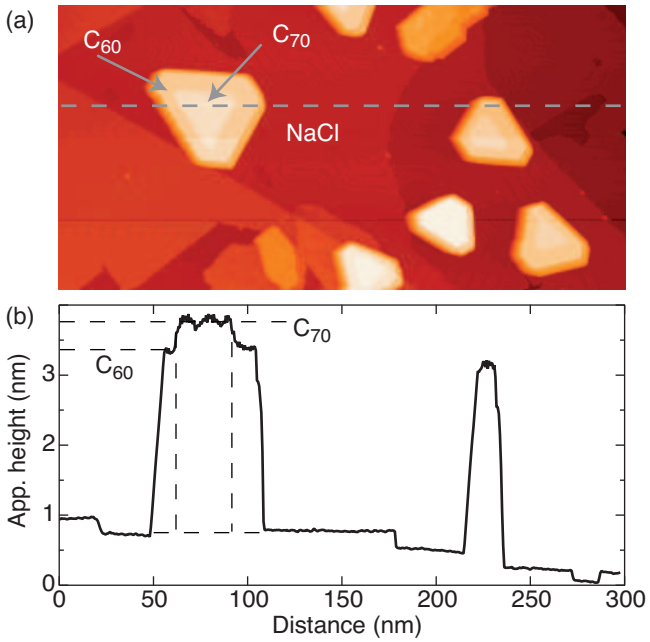

FIG. 11: (color online)(a) STM image of the surface topography resulting from successive depositions of C_{70} and C_{60} molecules, respectively, onto a NaCl/Au(111) substrate at 300 K. Tunneling parameters: $V = -3$ V; $I = 20$ pA. (b) Line profile taken along the line drawn in (a). The composition of of the left fullerene nanocrystal is indicated by vertical and horizontal dashed lines. The central part consist of only C_{70} molecules while the rim is composed exclusively of C_{60} molecules.

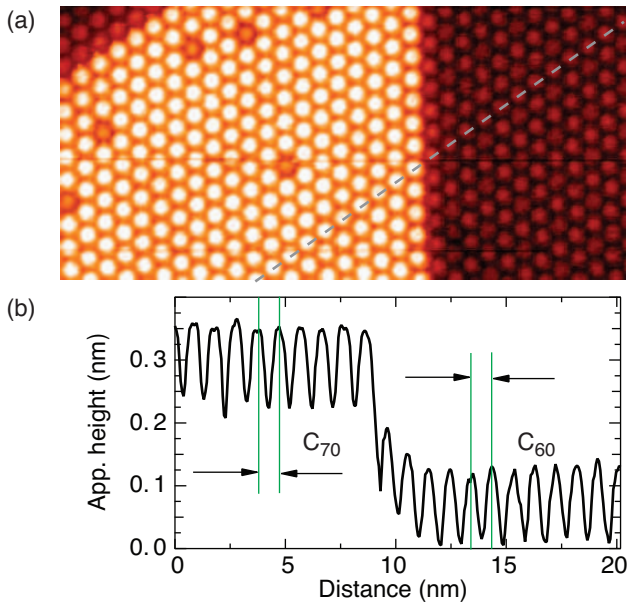

FIG. 12: (color online)(a) Submolecular resolution STM image revealing unoccupied molecular orbitals of fullerene molecules in the surface layer of the nanocrystal shown in Fig. 11(a). The nanoscale crystal exhibits a central part composed only of C_{70} molecules (bright contrast) and a rim, seen in the upper left part and in the right part of the image, formed only by C_{60} molecules (dark contrast). (b) Line profile taken along the line drawn in (a). The nearest-neighbor distance is 1.05 nm. Tunneling parameters: $V = +2.5$ V; $I = 0.02$ nA.

only one type of molecules. These results indicate that, as expected, each surface area of identical molecules maintains its intrinsic molecular arrangement.

2. *Simultaneous co-deposition*

Figure 13(a) shows a typical STM image of the surface topography after simultaneous depositions of C_{70} and C_{60} with a C_{60} concentration of about 75% onto NaCl covered Au(111) substrate. Deposition with a C_{60} concentration of about 50% yields similar results. The shape of the obtained mixed nanocrystals is similar to the one of the nanocrystals composed of only one species, i.e., truncated triangular or hexagonal. As can be inferred from the line profile displayed in Fig. 13(b), the nanocrystal shown in the STM image has a height of two molecular layers (2.05 ± 0.2 nm). In contrast to fullerene nanocrystals composed of only one type of molecules, the surface corrugation is high (approximately 0.2 nm) and non-periodic, owing to the presence of the two fullerene species, as shown in Fig. 14(a) and (b).

The two high resolution STM images of a mixed fullerene surface layer (see Fig. 13(a) and Fig. 14(a)) layer shown in Fig. 15(a) and (b) reveal unoccupied and occupied molecular orbitals, respectively. Also in the present case, the fullerene molecules form a hexagonal pattern despite the presence of two kinds of molecules. C_{60} and C_{70} molecules are distinguishable by their characteristic molecular orbitals. A comparison between the high resolution STM images and DFT calculations for the lowest unoccupied molecular orbital (see Fig. 15(c, bottom panel, central row)) and highest occupied molecular orbital (see Fig. 15(c, bottom panel, bottom row)) of the free C_{70} molecule allows us to identify the orientation of the molecules with respect to the surface plane. C_{70} molecules occupy random positions in this structure, exhibiting occasionally their long axis aligned parallel to the surface plane. For example, in Fig. 15(a), (b), (c, bottom right panel), the observed and calculated patterns of the molecular orbitals indicate that the C_{70} molecule *h:h* marked with a white square is facing the STM tip with its two hexagons. Note, however, that the observed lying C_{70} molecules may be rotated by different angles about their long axis. These high resolution images of the fullerenes together with the DFT calculations allow us to unambiguously identify the chemical nature and the orientation of each individual fullerene molecule within the surface layer of a mixed C_{60}/ C_{70} nanocrystal grown on NaCl.

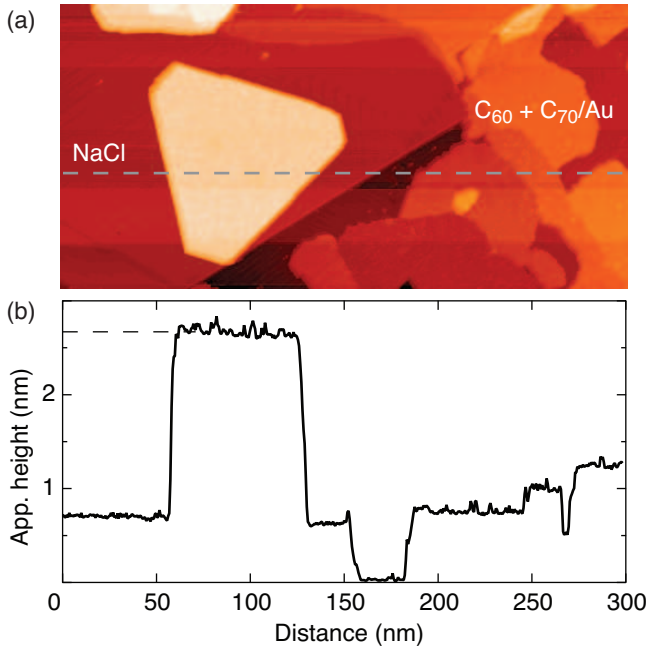

FIG. 13: (color online) a) STM image showing the growth of a C_{60}-C_{70} mixture on Au(111) and on NaCl/Au(111). b) Line profile corresponding to the dashed line in a). The nanocrystal has a height of two molecular layers (2.05 ± 0.2 nm).

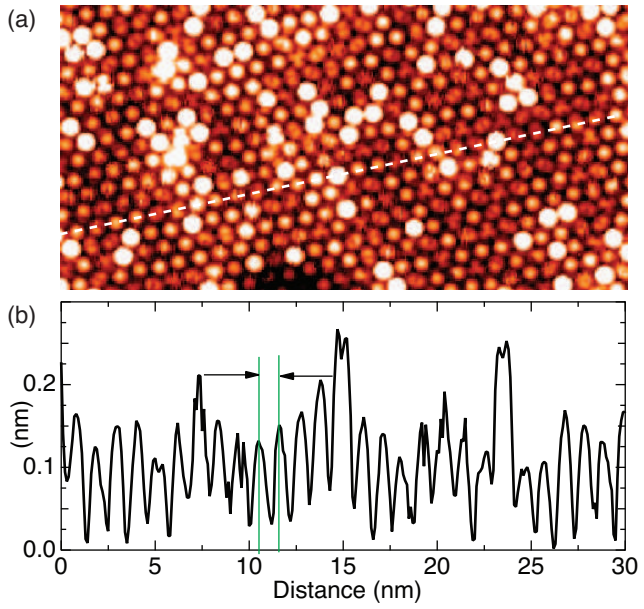

FIG. 14: (color online) a) Close-up view of the surface layer of a C_{60}-C_{70} nanocrystal, showing the close-packed arrangement of the molecules. b) Line profile corresponding to the dashed line in (a). The average nearest-neighbor distance is 1.05 nm. Tunneling parameters: $V = 2$ V, $I = 20$ pA.

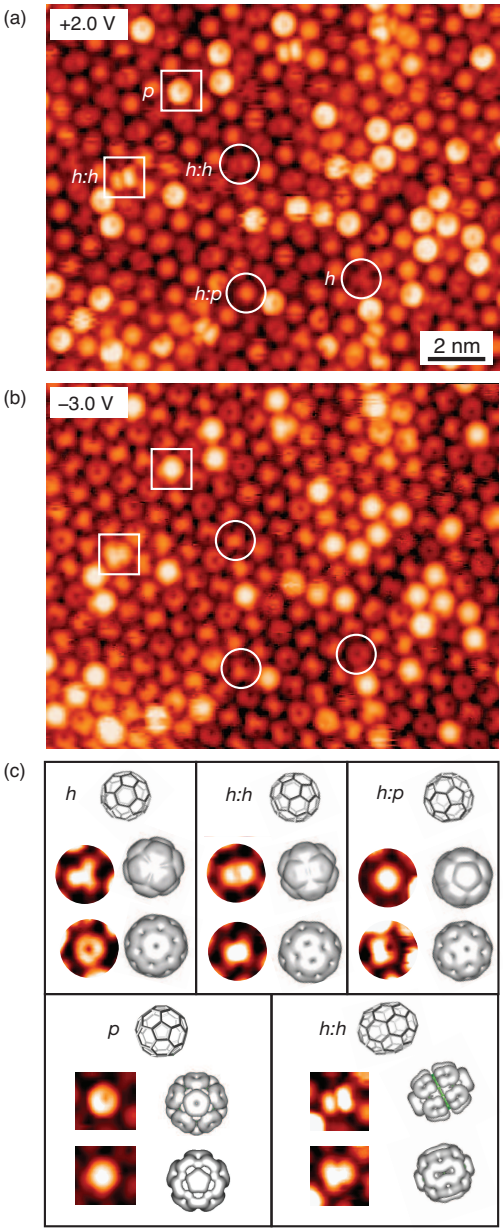

FIG. 15: (color online) (a, b)High-resolution STM images revealing unoccupied (a) and occupied (b) molecular orbitals of fullerene molecules on the surface layer of a mixed $C_{60}-C_{70}$ nanocrystal. c) Top panel, top row: Corresponding molecular orientations for C_{60} molecules with hexagon (h), hexagon–hexagon (h:h) and hexagon-pentagon (h:p) facing the STM tip. Top panel, second and third row: Comparison of the STM topography of single molecules (high-lighted by white circles in (a, b)) with DFT calculations for the lowest unoccupied (LUMO) and highest occupied (HOMO) molecular orbitals of free C_{60} molecules, respectively. Adapted from Fig. 6(c)). Bottom panel, top row: Corresponding molecular orientations for C_{70} molecules with pentagon (p) (long molecular axis perpendicular to surface plane) and hexagon–hexagon (h:h) (long molecular axis parallel to surface plane) facing the STM tip. Bottom panel, second and third row: Comparison of the STM topography of single molecules (high-lighted by white squares in (a, b)) with DFT calculations for the lowest unoccupied (LUMO) and highest occupied (HOMO) molecular orbitals of free C_{70} molecules, respectively. Tunneling parameters: (a) $V = +2$ V, $I = 20$ pA; (b) $V = -3$ V, $I = 20$ pA.

IV. SUMMARY

We have reported on the nucleation and growth of fullerenes on NaCl layers deposited on a Au(111) surface. We found that on the NaCl layers, the typical growth mode to form nanocrystals is different from the one reported from fullerene growth on bare metal substrates, an observation which seems to be quite general for the growth of organic molecules on dielectric materials. This specific growth behavior on dielectric ultrathin films indicates that the inter-molecular interactions are stronger than the molecule-dielectric film interactions. Evidently, the dielectric film reduces the wave function overlap between the molecular frontier orbitals and the wave functions of the underlying metallic substrate, supporting the dielectric film. Both, C_{60} and C_{70} molecules as well as mixtures of both species form truncated triangular or hexagonal nanocrystals with a height of several molecular layers upon adsorption on a NaCl covered Au(111) substrate. The nucleation sites of the nanocrystals are NaCl covered Au(111) steps, defects of the NaCl film and step edges of multilayer islands of NaCl on ultrathin NaCl films. High resolution STM images combined with DFT calculations for the LUMO and HOMO molecular orbitals show that C_{60} and C_{70} tend to arrange in a configuration in which electron-poor regions on one molecule face electron-rich regions on the adjacent molecule. These findings allow us to unambiguously identify the chemical nature and the orientation of each individual fullerene molecule within the surface layer of a mixed C_{60}/ C_{70} nanocrystal grown on NaCl. Moreover, these tools allowed us to detect long-range orientational order in the the surface layer of genuine C_{60} and C_{70} nanocrystals. We note that these types of nanocrystals have been extremely useful for STM induced light emission experiments in order to determine the ultimate spatial resolution of this technique obtainable from an ensemble of organic molecules[64,65].

V. ACKNOWLEDGMENTS

Financial support from the Swiss National Science Foundation is acknowledged.

[1] H. M. Kroto, J. R. Heath, S. C. O'Brien, R. F. Curl, and R. E. Smalley, Nature **318**, 162 (1985).

[2] M. S. Dresselhaus, G. Dresselhaus, and P. C. Eklund, *Science of Fullerenes and Carbon Nanotubes* (Academic Press, New York, 1996).

[3] G. Binnig and H. Rohrer, Rev. Mod. Phys. **59**, 615 (1987).

[4] T. Hashizume, K. Motai, X. D. Wang, H. Shinohara, Y. Saito, Y. Maruyama, K. Ohno, Y. Kawazoe, Y. Nishina, H. W. Pickering, et al., Phys. Rev. Lett. **71**, 2959 (1993).

[5] J. K. Gimzewski, S. Modesti, T. David, and R. R. Schlittler, J. Vac. Sci. Techn. **12**, 1942 (1994).

[6] C. Rogero, J. I. Pascual, J. Gomez-Herrero, and A. M. Baro, J. Chem. Phys. **116**, 832 (2002).

[7] E. I. Altman and R. J. Colton, Phys. Rev. B **48**, 18244 (1993).

[8] E. I. Altman and R. J. Colton, Surf. Sci. **295**, 13 (1993).

[9] R. Gaisch, R. Berndt, J. Gimzewski, B. Reihl, R. Schlittler, W.-D. Schneider, and M. Tschudy, Appl. Phys. A **57**, 207 (1993).

[10] G. Schull and R. Berndt, Phys. Rev. Lett. **99**, 226105 (2007).

[11] B. W. Hoogenboom, R. Hesper, L. H. Tjeng, and G. A. Sawatzky, Phys. Rev. B **57**, 11939 (1998).

[12] X. Lu, M. Grobis, K. H. Khoo, S. G. Louie, and M. F. Crommie, Phys. Rev. B **70**, 115418 (2004).

[13] C. T. Tzeng, W. S. Lo, R. Y. Yuh, and K. D. Tsuei, Phys. Rev. B **61**, 2263 (2000).

[14] T. R. Ohno, Y. Chen, S. E. Harvey, G. H. Kroll, J. H. Weaver, R. E. Haufler, and R. E. Smalley, Phys. Rev. B **44**, 13747 (1991).

[15] Y. Z. Li, J. C. Patrin, M. Chander, J. H. Weaver, L. P. F. Chibante, and R. E. Smalley, Science **252**, 547 (1991).

[16] R. Schwedhelm, J.-P. Schlomka, S. Woedtke, R. Adelung, L. Kipp, M. Tolan, W. Press, and M. Skibowski, Phys. Rev. B **59**, 13394 (1999).

[17] M. Grobis, X. Lu, and M. F. Crommie, Phys. Rev. B **66**, 161408 (2002).

[18] I. F. Torrente, K. J. Franke, and J. I. Pascual, J. Phys.: Condens. Matter **20**, 184001 (2008).

[19] S. A. Burke, J. M. Mativetsky, R. Hoffmann, and P. Grütter, Phys. Rev. Lett. **94**, 096102 (2005).

[20] S. A. Burke, J. M. Mativetsky, S. Fostner, and P. Grutter, Phys. Rev. B **76**, 035419 (2007).

[21] S. A. Burke, J. M. Topple, and P. Gruetter, J. Phys. - Condens. Matter **21** (2009).

[22] M. Cañas-Ventura, W. Xiao, P. Ruffieux, R. Rieger, K. Müllen, H. Brune, and R. Fasel, Surface Science **603**, 2294 (2009), ISSN 0039-6028.

[23] L. Ramoino, M. von Arx, S. Schintke, A. Baratoff, H. J. Guntherodt, and T. A. Jung, Chem. Phys. Lett. **417**, 22 (2006).

[24] Y. Wang, J. Kröger, R. Berndt, and H. Tang, J. Am. Chem. Soc. **132**, 12546 (2010).

[25] E. Ćavar, Ph.D. thesis, École Polytechnique Fédérale de Lausanne (2005).

[26] F. Rossel, Ph.D. thesis, École Polytechnique Fédérale de Lausanne (2009).

[27] R. Gaisch, J. K. Gimzewski, B. Reihl, R. R. Schlittler, M. Tschudy, and W.-D. Schneider, Ultramicroscopy **42-44**, 1621 (1992).

[28] CPMD, *Copyright IBM Corp 1990-2008 and Copyright MPI für Festkörperforschung Stuttgart 1997-2001*, http://www.cpmd.org.

[29] C. Adamo and V. Barone, J. Chem.Phys. **110**, 6158 (1999).

[30] P. Giannozzi, S. Baroni, N. B. M. Calandra, R. Car, C. Cavazzoni, D. Ceresoli, G. L. Chiarotti, M. Cococcioni, I. Dabo, A. D. Corso, et al., J. Phys.: Condensed Matter **21**, 395502 (2009).

[31] T. Thonhauser, V. Cooper, S. Li, A. Puzder, P. Hyldgaard, and D. Langreth, Phys. Rev. B **76**, 125112 (2007).

[32] E. Ćavar, M.-C. Blüm, M. Pivetta, F. Patthey, M. Chergui, and W.-D. Schneider, Phys. Rev. Lett. **95**, 196102 (2005).

[33] J. V. Barth, H. Brune, G. Ertl, and R. J. Behm, Phys. Rev. B **42**, 9307 (1990).

[34] F. Rossel, P. Brodard, F. Patthey, N. V. Richardson, and W. D. Schneider, Surf. Sci. **602**, L115 (2008).

[35] C. Schwennicke, J. Schimmelpfennig, and H. Pfnür, Surf. Sci. **293**, 57 (1993).

[36] W. Hebenstreit, J. Redinger, Z. Horozowa, M. Schmid, R. Podloucky, and P. Varga, Surf. Sci. **424**, L321 (1999).

[37] W. Hebenstreit, M. Schmid, J. Redinger, R. Podloucky, and P. Varga, Phys. Rev. Lett. **85**, 5376 (2000).

[38] X. Sun, M. P. Felicissimo, P. Rudolf, and F. Silly, Nanotechnology **19**, 495307 (5pp) (2008).

[39] K. Yase, N. Ara-Kato, T. Hanada, H. Takiguchi, Y. Yoshida, G. Back, K. Abe, and N. Tanigaki, Thin Solid Films. **331**, 131 (1998).

[40] P. A. Heiney, J. E. Fischer, A. R. McGhie, W. J. Romanow, A. M. Denenstein, J. P. McCauley, A. B. Smith, and D. E. Cox, Phys. Rev. Lett. **66**, 2911 (1991).

[41] R. Sachidanandam and A. B. Harris, Phys. Rev. Lett. **67**, 1467 (1991).

[42] E. J. J. Groenen, O. G. Poluetkov, M. Matushita, J. Schmidt, J. H. Van Der Waals, and G. Meijer, Chem. Phys. Lett. **197**, 314 (1992).

[43] J. E. Fischer and P. A. Heiney, J. Phys. Chem. Solids **54**, 1725 (1993).

[44] W. I. F. David, R. M. Ibberson, T. J. S. Dennis, J. P. Hare, and K. Prassides, Europhys. Lett. **18**, 219 (1992).

[45] W. I. F. David, R. M. Ibberson, J. C. Matthewman, K. Prassides, T. J. S. Dennis, J. P. Hare, H. W. Kroto, R. Taylor, and D. R. M. Walton, Nature **353**, 147 (1991).

[46] W. I. F. David, R. M. Ibberson, and T. Matsuo, Proc. R. Soc. London Ser. A **442**, 129 (1993).

[47] G. Van Tendeloo, S. Amelinckx, M. A. Verheijen, P. H. M. van Loosdrecht, and G. Meijer, Phys. Rev. Lett. **69**, 1065 (1992).

[48] H. Q. Wang, C. G. Zeng, B. Wang, J. G. Hou, Q. X. Li, and J. L. Yang, Phys. Rev. B **63**, 085417 (2001).

[49] E. I. Altman and R. J. Colton, Surf. Sci. **279**, 49 (1992).

[50] S. Behler, H. P. Lang, S. H. Pan, V. Thommen-Geisser, and H. J. Guntherodt, Z. Phys. B **91**, 1 (1993).

[51] R. Gaisch, R. Berndt, W.-D. Schneider, J. K. Gimzewski, B. Reihl, R. R. Schlittler, and M. Tschudy, J. Vac. Sci. Technol. **12**, 2153 (1994).

[52] X. Lu, M. Grobis, K. H. Khoo, S. G. Louie, and M. F. Crommie, Phys. Rev. Lett. **90**, 096802 (2003).

[53] K. Prassides, H. W. Kroto, R. Taylor, D. R. M. Walton, W. I. F. David, J. Tomkinson, R. C. Haddon, M. J. Rosseinsky, and D. W. Murphy, Carbon **30**, 1277 (1992).

[54] M. A. Verheijen, H. Meekes, G. Meijer, P. Bennema, J. L. Deboewr, S. van Smaalen, G. van Tendeloo, S. Amelinckx, S. Muto, and J. van Landuyt, Chem. Phys. **166**, 287 (1992).

[55] G. B. M. Vaughan, P. A. Heiney, D. E. Cox, J. E. Fischer, A. R. McGhie, A. L. Smith, R. M. Strongin, M. A. Cichy, and A. B. Smith, Chem. Phys. **178**, 599 (1993).

[56] G. van Tendeloo, S. Amelinckx, J. L. Deboer, S. van Smaalen, M. A. Verheijen, H. Meekes, and G. Meijer, Europhys. Lett. **21**, 329 (1993).

[57] M. A. Verheijen, M. S. Couto, K. W. M. Koutstaal, and W. J. P. van Enckevort, Philos. Mag. A **72**, 1141 (1995).

[58] G. B. M. Vaughan, P. A. Heiney, J. E. Fischer, D. E. Luzzi, D. A. Ricketts-Foot, A. R. McGhie, Y. W. Hui, A. L. Smith, D. E. Cox, W. J. Romanniw, et al., Science **254**, 1350 (1991).

[59] M. C. Valsakumar, N. Subramanian, M. Yousuf, P. C. Sahu, Y. Hariharan, A. Bharathi, V. Sankara Sastry, J. Janaki, G. V. N. Rao, T. S. Radhakrishnan, et al., Phys. Rev. B **48**, 9080 (1993).

[60] J. Shumway and S. Satpathy, Chem. Phys. Lett. **211**, 595 (1993).

[61] J. K. Gimzewski, T. A. Jung, M. T. Cuberes, and R. R. Schlittler, Surf. Sci. **386**, 101 (1997).

[62] M. de Wild, S. Berner, H. Suzuki, H. Yanagi, D. Schlettwein, S. Ivan, A. Baratoff, H.-J. Guentherodt, and T. A. Jung, ChemPhysChem **10**, 881 (2002).

[63] H. Spillmann, A. Kiebele, M. Stöhr, T. A. Jung, D. Bonifazi, F. Cheng, and F. Diederich, Adv. Mat. **18**, 275 (2006).

[64] F. Rossel, M. Pivetta, F. Patthey, and W. D. Schneider, Opt. Express **17**, 2714 (2009).

[65] F. Rossel, M. Pivetta, and W. D. Schneider, Surf. Sci. Rep. **65**, 129 (2010).